



Slip Boundary Conditions in Ballistic–Diffusive Heat Transport in Nanostructures

Yu-Chao Hua and Bing-Yang Cao

Department of Engineering Mechanics, Key Laboratory for Thermal Science and Power Engineering of Ministry of Education, Tsinghua University, Beijing, P. R. China

ABSTRACT

Ballistic–diffusive heat conduction, which is predominantly affected by boundaries and interfaces, will occur in nanostructures whose characteristic lengths are comparable to the phonon mean free path (MFP). Here, we demonstrated that interactions between phonons and boundaries (or interfaces) could lead to two kinds of slip boundary conditions in the ballistic–diffusive regime: boundary temperature jump and boundary heat flux slip. The phonon Boltzmann transport equation (BTE) with relaxation time approximation and the phonon tracing Monte Carlo (MC) method were used to investigate these two slip boundary conditions for the ballistic–diffusive heat conduction in nanofilms on a substrate. For cross-plane heat conduction where the boundary temperature jump is the dominant non-Fourier phenomenon, ballistic transport causes the temperature jumps and thus introduces a ballistic thermal resistance. Importantly, when considering the interface effect, the corresponding model was derived based on the phonon BTE and verified by comparing with the MC simulations. In addition, an interface–ballistic coupling effect was identified, which indicates inapplicability of the standard thermal resistance analysis. In contrast, for the in-plane case that is controlled by boundary heat flux slip, both phonon boundary scattering and perturbation of the phonon distribution function induced by the interface can cause heat flux slip, leading to a variation in in-plane thermal resistance. In addition, a model beyond the Fuchs–Sondheimer formula, which can address both the boundary scattering and the interface effects, was derived based on the phonon BTE. The good agreements with the MC simulations indicate its validity.

ARTICLE HISTORY


Received 6 May 2017
Accepted 16 June 2017

KEYWORDS

Ballistic–diffusive heat conduction; slip boundary condition; phonon Boltzmann transport equation; Monte Carlo

Introduction

Rapid development of nanotechnologies necessitates an in-depth understanding of nanoscale thermal transport [1, 2]. In nanostructures whose characteristic lengths are comparable to the phonon mean free path (MFP), thermal transport could significantly deviate from the prediction based on Fourier's law, leading to ballistic–diffusive heat conduction [2]. Boundaries and interfaces dominate phonon transport in the ballistic–diffusive regime, and most of the non-Fourier phenomena in this case could be attributed to phonon–boundary (or interface) interactions [2–5]. Therefore, the study on boundary conditions is essentially important for a better understanding of ballistic–diffusive heat conduction, and it can also provide an efficient way to characterize nanoscale thermal transport by using the classical Fourier's law modified with slip boundary conditions [6–10].

CONTACT Bing-Yang Cao  caoby@mail.tsinghua.edu.cn  Department of Engineering Mechanics, Key Laboratory for Thermal Science and Power Engineering of Ministry of Education, School of Aerospace Engineering, Tsinghua University, Beijing 100084, P. R. China.

Color versions of one or more of the figures in the article can be found online at www.tandfonline.com/umte.

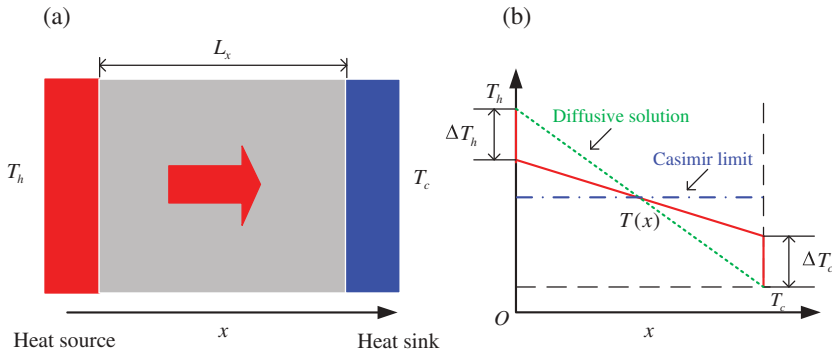


Figure 1. (a) Schematic diagram of cross-plane heat conduction in a nanofilm: a nanofilm with x -directional length, L_x , in contact with two phonon baths of temperatures T_h and T_c ; (b) temperature jumps, ΔT_h and ΔT_c , occur at the boundaries.

As is well known, slip boundary conditions have been extensively investigated in fluid mechanics [11]. In addition, in the ballistic–diffusive heat conduction, the interactions between phonons and boundaries cause two types of slip boundary conditions: boundary temperature jump [12–16] and boundary heat flux slip [17–20]. As shown in Figure 1, in the diffusive regime, the boundary temperature should be equal to the temperature of the contacted phonon bath, whereas in the ballistic–diffusive regime, a difference between the boundary temperature and the phonon bath temperature could exist, called the boundary temperature jump [6, 7]. Some works have been conducted on the temperature jumps at the ideal and reflectionless boundary (i.e., the phonon black-body boundary) [6, 7, 15]. Hua and Cao [6] used the differential approximation method to derive the boundary temperature jump model in this case, and they found that the boundary temperature jump is proportional to both the phonon MFP and the local temperature gradient. In addition, Maassen and Lundstrom [7, 8] obtained a similar formula for the boundary temperature jump by using the McKelvey-Shockley flux method. The work of Sellan et al. [15] demonstrated that the boundary temperature jumps could cause a reduction in effective thermal conductivities and thus increase the total thermal resistance. In fact, there is one critical issue about the boundary temperature jumps that still remains unclarified; that is, the interface effect, which usually exists at boundaries. For example, Wilson and Cahill [21] proposed that the interfacial resistance and ballistic effect could be coupled, which plays an important role in time-domain thermoreflectance experiments where a metal film transducer is needed.

Additionally, for a purely diffusive heat conduction process, Fourier’s law will predict a uniform heat flux distribution in the case as shown in Figure 2, because no temperature gradient exists in the

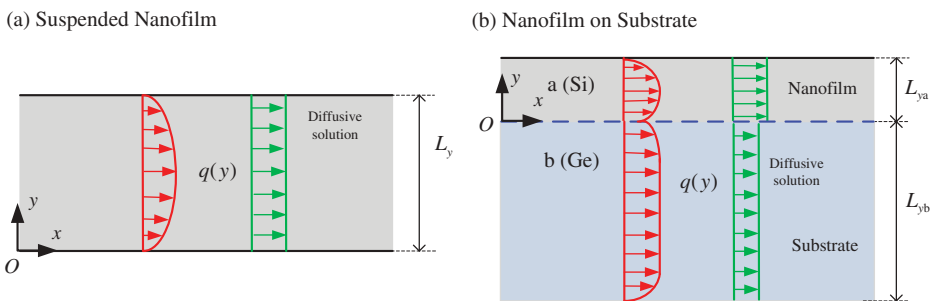


Figure 2. (a) Schematic diagram of boundary heat flux slip in a suspended in-plane nanofilm: the y -directional thickness is L_y , and the heat flux $q(y)$ along the x -direction varies in the y -direction; (b) schematic diagram of boundary heat flux slip in an in-plane nanofilm labeled “a” on a substrate labeled by “b”: the nanofilm thickness is L_{ya} , the substrate thickness is L_{yb} , and $L_{ya} < L_{yb}$.

lateral direction. On the contrary, in the ballistic–diffusive regime, the heat flux near the lateral boundaries (or interfaces) could be influenced by the phonon–boundary (or interfaces) interactions, called boundary heat flux slip [18, 20]. Ziman [22] derived the heat flux distribution formulas for suspended films and wires based on the phonon Boltzmann transport equation (BTE) and found that the heat flux is reduced near the boundaries due to the diffusive phonon–boundary scattering. In addition, in the theoretical frame of phonon hydrodynamics, Sellitto et al. [18] proposed a phenomenological boundary heat flux slip model analogous to the well-known velocity slip boundary condition model in fluid mechanics. The roughness and interface significantly influence the boundary heat flux slip. In Ziman’s [22] pioneering work, the influence of boundary roughness was characterized using a specular parameter. Martin et al. [23] employed perturbation theory to compute the frequency-dependent phonon–boundary scattering rate, which depends on the root mean square roughness height and autocovariance length. In practice, a nanofilm cannot always be suspended, and the existence of a substrate (i.e., interface) leads to perturbation of the phonon distribution function and thus has an influence on the heat flux distribution [24, 25]. Several researchers have discussed this substrate effect on the thermal conductivity of some single-layer or multiple-layer two-dimensional materials [26–28], though its influence on heat flux distribution requires more in-depth investigation and, importantly, a reliable predictive model considering substrate effects is still lacking.

In the present work, we analyzed the slip boundary conditions for ballistic–diffusive heat conduction in nanofilms on a substrate, which have been widely utilized in electronic devices [1]. The phonon BTE with relaxation time approximation was used to derive the corresponding analytical models. A phonon tracing Monte Carlo (MC) technique was used to simulate the phonon transport for comparison with the derived theoretical models. Generally, thermal transport in nanofilms can be clarified into two typical types; that is, cross-plane heat conduction and in-plane heat conduction. Boundary temperature jump is the dominant non-Fourier phenomenon for the cross-plane case, whereas the in-plane case is controlled by boundary heat flux slip. Here, we highlight the interface effects on these two slip boundary conditions, which have not been well clarified in the previous works. A more in-depth understanding as well as analytical models of the ballistic–interface coupling effects in ballistic–diffusive heat conduction have been provided, which could be helpful for predicting and controlling thermal transport in nanostructures.

Methodology

The phonon BTE with relaxation time approximation is given by [2, 22]

$$\vec{v}_{g\omega} \cdot \nabla f_{\omega} = \frac{f_{0\omega} - f_{\omega}}{\tau_{\omega}}, \quad (1)$$

where ω is the angular frequency, $\vec{v}_{g\omega}$ is the group velocity, f_{ω} is the phonon distribution function, $f_{0\omega}$ is the equilibrium distribution function, and τ_{ω} is the relaxation time. In order to verify our derived theoretical models, a phonon tracing MC method [29–31] has been used to simulate phonon transport process in nanofilms, which is equivalent to numerically solving the phonon BTE. This technique is able to handle problems with complicated geometries as well as multiple scattering events and transient heat conduction processes. Péraud and Hadjiconstantinou [29] and Hua and Cao [30] used it to investigate the heat conduction in various nanostructures, including nanofilms, nanowires, and nanoporous materials, and it has been found that the phonon tracing MC simulations well predict the results by both theoretical models and experiments. In addition, Tang et al. [31] used this technique to simulate the ultrafast heat conduction in nanostructures, in which ballistic effects could be coupled with heat wave effects.

The trajectories of individual phonons are simulated independently in the phonon tracing MC simulation. Basically, it includes six procedures [30]:

- (1) Input phonon properties and set the total number of phonon bundles.
- (2) Draw the initial properties of the phonon bundle according to the nature of emitting boundaries (these properties, including initial position, traveling direction, angular frequency, etc., are determined by random number samplings).
- (3) Calculate the traveling length until the first scattering event and renew the position of phonon bundles.
- (4) When a phonon bundle collides with a boundary, renew the phonon bundle position at the boundary (if the boundary is nonabsorbing or adiabatic, the phonon bundle should be reflected back into the domain).
- (5) If a phonon bundle does not collide with boundaries, the phonon bundle should be reemitted within the media, and the tracing process then proceeds to (c).
- (6) If the phonon bundle arrives at an absorbing boundary, the tracing process of this phonon bundle is finished, and the simulation then proceeds to (b) and then begins the tracing process of the next phonon bundle.

Boundary temperature jump

Boundary temperature jump at ideal and reflectionless boundary

We begin by analyzing the boundary temperature jump in cross-plane heat conduction. As shown in [Figure 1](#), the cross-plane nanofilm is in contact with the phonon baths of temperatures T_h and T_c , respectively. The boundaries are firstly assumed to be ideal and reflectionless (i.e., phonon black-body) [6, 7] and thus the phonons arriving at the boundaries will be absorbed. Consider the boundary condition at $x = 0$. Due to the law of conservation of energy, the heat flux at the boundary should be continuous; that is,

$$q_x = q_x^+ - q_x^-, \quad (2)$$

where q_x is the net heat flux, and q_x^+ and q_x^- are the positive and negative directional heat fluxes, respectively. The net heat flux is calculated as

$$q_x = \int_0^{2\pi} d\varphi \int_{-1}^1 \mu d\mu \int \hbar\omega v_g D(\omega) d\omega f_\omega, \quad (3)$$

in which φ is the azimuthal angle, $\mu = \cos(\theta)$ in which θ is the polar angle between the phonon traveling direction and the x -axis, \hbar is the Dirac constant, and $D(\omega)$ is the density of states. The negative directional heat flux is

$$q_x^- = - \int_0^{2\pi} d\varphi \int_{-1}^0 \mu d\mu \int \hbar\omega v_g D(\omega) d\omega f_\omega. \quad (4)$$

The positive heat flux, which depends on the properties of the phonon bath, can be expressed as

$$q_x^+ = \int_0^{2\pi} d\varphi \int_0^1 \mu d\mu \int \hbar\omega v_g D(\omega) d\omega f_{0\omega}(T_h). \quad (5)$$

According to Hua and Cao [6], the phonon BTE can be simplified by differential approximation [32]; that is,

$$f_\omega = f_{0\omega} - v_{g\omega} \tau_\omega \mu \frac{\partial f_{0\omega}}{\partial x}, \quad (6)$$

which considers the first-order deviation from local equilibrium. It is noted that the differential approximation alone could fail when the ballistic effect becomes significant [9], though several works [6–8] have already demonstrated that the differential approximation, which is also equivalent to the McKelvey-Shockley flux approach [7], could well predict the ballistic–diffusive thermal transport once the boundary conditions are properly specified.

For simplicity and clarity, the gray approximation is adopted and thus we have [32]

$$\frac{\partial [\int \hbar \omega v_{g\omega} D(\omega) d\omega f_{0\omega}(T)]}{\partial T} = \frac{C_V v_g}{4\pi}, \quad (7)$$

where C_V is the heat capacity and v_g is the average group velocity. Then, combining Eqs. (3), (6), and (7), the net heat flux is given by

$$q_x = -\frac{C_V v_g l_0}{3} \frac{\partial T}{\partial x}, \quad (8)$$

where $l_0 = v_g \tau$ is the average phonon MFP, and $k_0 = C_V v_g l_0 / 3$ is the benchmarked thermal conductivity. Under the differential approximation, the net heat flux can be characterized by the classical Fourier's law, because the leading first-order deviation can be eliminated via the integral over the whole solid angle space within the medium. The ballistic effect mainly occurs at boundaries and thus a proper slip boundary condition should be important in this case. Then, using Eqs. (4), (5), and (6), we have

$$q_x^- = \frac{C_V v_g T}{4} + \frac{C_V v_g l_0}{6} \frac{\partial T}{\partial x}, \quad (9)$$

$$q_x^+ = \frac{C_V v_g T_h}{4}. \quad (10)$$

In terms of the continuous condition of boundary heat flux, Eq. (2), the temperature jump at $x = 0$ is given by

$$T_h - T|_0 = -\frac{2l_0}{3} \frac{\partial T}{\partial x} \Big|_0 = \frac{2}{C_V v_g} q_x|_0. \quad (11)$$

Furthermore, following similar procedures, the boundary temperature jump condition at $x = L$ can be obtained:

$$T|_{L_x} - T_c = -\frac{2l_0}{3} \frac{\partial T}{\partial x} \Big|_{L_x} = \frac{2}{C_V v_g} q_x|_{L_x}. \quad (12)$$

Combining Eqs. (8), (11), and (12) yields the temperature distribution within the nanofilms,

$$T(x) = \frac{\left[T_h + (T_c - T_h) \frac{x}{L_x} \right] + \frac{2}{3} Kn_x (T_c + T_h)}{1 + \frac{4}{3} Kn_x}, \quad (13)$$

in which $Kn_x = l_0 / L_x$ is the Knudsen number. As $Kn_x \rightarrow 0$, Eq. (13) is reduced to the completely diffusive solution, $T(x) = T_c + (T_h - T_c)x / L_x$; as $Kn_x \rightarrow \infty$, Eq. (13) becomes $T(x) = (T_h + T_c) / 2$,

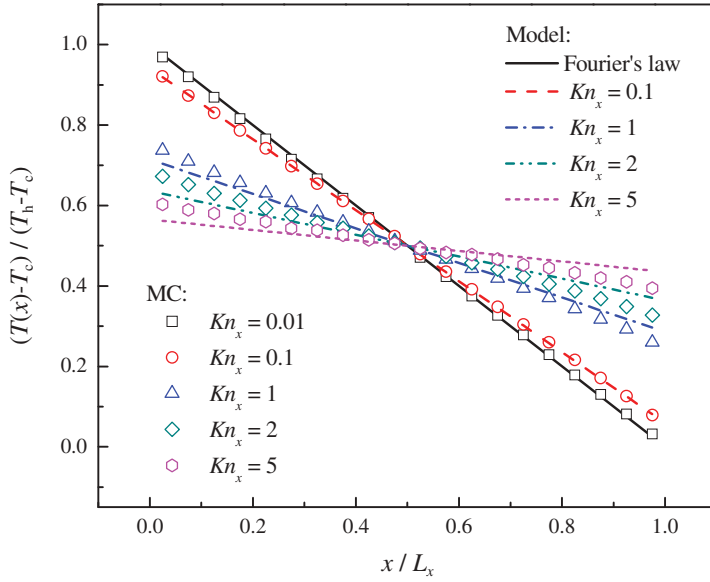


Figure 3. Temperature distributions in cross-plane nanofilms with ideal and reflectionless boundaries.

which is the Casimir limit [13] in the purely ballistic regime. Figure 3 shows the temperature distributions in cross-plane nanofilms with ideal and reflectionless boundaries. When $Kn_x = 0.01$, the ballistic transport effect is negligible and thus Fourier’s law well predicts the temperature profile obtained by the MC simulations. With increasing Knudsen number, Kn_x , the boundary temperature jumps occur and increase, leading to a deviation from Fourier’s law, though the temperature profiles are still linear within the nanofilms. In addition, the results predicted by Eq. (13) agree well with those by MC simulations, especially when the Knudsen number is small. Due to the differential approximation, a slight deviation (about 5%) could occur as the Knudsen number increases.

Additionally, according to Eqs. (8) and (13), we can obtain the cross-plane thermal resistance of the nanofilms,

$$R_{cr} = \frac{L_x}{k_0} \left(1 + \frac{4}{3} Kn_x \right) = R_0 + R_{ball}, \quad (14)$$

in which $R_0 = L_x/k_0$ is the benchmark thermal resistance calculated by the classical Fourier’s law, and $R_{ball} = 4/(v_g C_V)$ is the ballistic thermal resistance [7, 33]. Figure 4 shows the cross-plane thermal resistances calculated by the model and MC simulations, respectively. The boundary temperature jumps reduce the effective temperature difference imposed on the nanofilms, resulting in an increase in cross-plane thermal resistance; that is, a reduction in effective thermal conductivity. In addition, referring to Maassen and Lundstrom [7, 8], this phenomenon could be explained as the influence of the ballistic thermal resistance, which is enhanced as the Knudsen number increases. In addition, as reported in Hua and Cao [6, 16], Kaiser et al. [10], and Majumdar [13], the model Eq. (14) could be a fairly good approximation of the phonon BTE for cross-plane heat conduction in nanofilms with ideal boundaries; thus, it can well predict the results obtained by MC simulations, and the maximum deviation should be less than 5%.

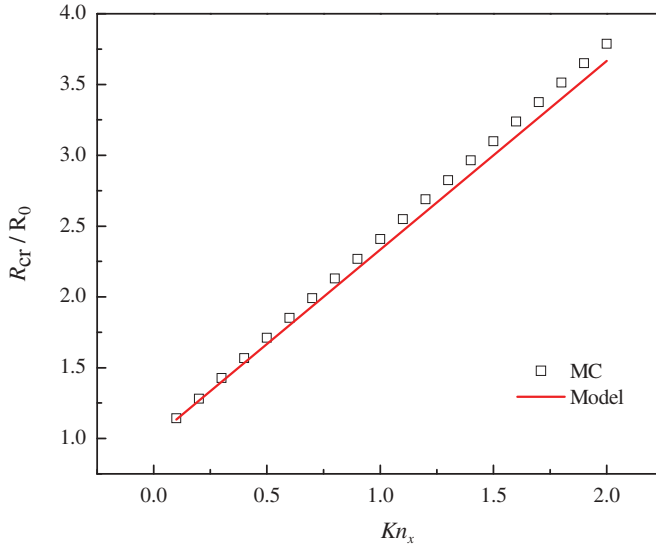


Figure 4. Cross-plane thermal resistance of nanofilms with ideal and reflectionless boundaries.

Boundary temperature jump with interface effect

An ideal and reflectionless boundary is not realistic in practice, because interfaces frequently exist at boundaries [21]. Therefore, the influence of the phonon property dissimilarity should be taken into account. Regarding this, the positive heat flux becomes

$$q_x^+ = \int_0^{2\pi} d\varphi \int_0^1 \mu d\mu \int \hbar \omega v_{gh} D(\omega) d\omega t_{hf} f_{0\omega}(T_h) - \int_0^{2\pi} d\varphi \int_{-1}^0 \mu d\mu \int \hbar \omega v_g D(\omega) d\omega r_{fh} f_{\omega}, \quad (15)$$

in which t_{hf} is the transmissivity from the heat sink to the film, and r_{fh} is the reflectivity back to the film. By using the differential approximation and the Debye approximation, Eq. (15) is rewritten as

$$q_x^+ = \frac{C_{vh} v_{gh} T_h}{2} \int_0^1 t_{hf} \mu d\mu - \frac{C_v v_g T}{2} \int_{-1}^0 r_{fh} \mu d\mu + \frac{C_v v_g l_0}{2} \frac{\partial T}{\partial x} \int_{-1}^0 r_{fh} \mu^2 d\mu. \quad (16)$$

At room temperature, the diffusive mismatch model (DMM) is frequently used to characterize the transmissivity and reflectivity at interfaces [34]. Then we have

$$t_{hf} = \frac{C_v v_g}{C_{vh} v_{gh} + C_v v_g}, \quad r_{fh} = \frac{C_v v_g}{C_{vh} v_{gh} + C_v v_g}, \quad (17)$$

in which C_{vh} and v_{gh} are the heat capacity and group velocity of heat sink material, respectively. Because t_{hf} and r_{fh} are independent of μ in the DMM, Eq. (16) is simplified as

$$q_x^+ = t_{hf} \frac{C_{vh} v_{gh} T_h}{4} + r_{fh} \frac{C_v v_g T}{4} + \frac{C_v v_g l_0}{6} r_{fh} \frac{\partial T}{\partial x}. \quad (18)$$

Combining Eqs. (2), (9), and (18) yields the boundary temperature jump at $x = 0$,

$$T_h \left(\frac{C_{vh} v_{gh}}{C_v v_g} \frac{t_{hf}}{1 - r_{fh}} \right) - T|_0 = -\frac{2}{3} l_0 \left(\frac{1 + r_{fh}}{1 - r_{fh}} \right) \frac{\partial T}{\partial x} \Big|_0 \Rightarrow T_h - T|_0 = -\frac{2}{3} l_0 \left(\frac{1 + r_{fh}}{1 - r_{fh}} \right) \frac{\partial T}{\partial x} \Big|_0. \quad (19)$$

In addition, following the same steps, we can derive the boundary temperature jump at $x = L$,

$$T|_L - T_c \left(\frac{C_{vc} v_{gc}}{C_v v_g} \frac{t_{cf}}{1 - r_{fc}} \right) = -\frac{2}{3} l_0 \left(\frac{1 + r_{fc}}{1 - r_{fc}} \right) \frac{\partial T}{\partial x} \Big|_L \Rightarrow T|_L - T_c = -\frac{2}{3} l_0 \left(\frac{1 + r_{fc}}{1 - r_{fc}} \right) \frac{\partial T}{\partial x} \Big|_L, \quad (20)$$

where the transmissivity t_{cf} and the reflectivity r_{fc} are also calculated by the DMM [29].

Then, combining Eqs. (8), (19), and (20) yields the temperature distribution within the nanofilms considering the interface effect; that is,

$$T(x) = \frac{\left[T_h + (T_c - T_h) \frac{x}{L_x} \right] + \frac{2}{3} Kn_x \left(\frac{1+r_{fh}}{1-r_{fh}} T_c + \frac{1+r_{fc}}{1-r_{fc}} T_h \right)}{1 + \frac{2}{3} Kn_x \left(\frac{1+r_{fh}}{1-r_{fh}} + \frac{1+r_{fc}}{1-r_{fc}} \right)}. \quad (21)$$

Similarly, as $Kn_x \rightarrow 0$, Eq. (21) is also reduced to the diffusive solution, $T(x) = T_c + (T_h - T_c)x/L_x$. In contrast, as $Kn_x \rightarrow \infty$, Eq. (21) becomes

$$T(x) = \frac{\frac{1+r_{fh}}{1-r_{fh}} T_c + \frac{1+r_{fc}}{1-r_{fc}} T_h}{\frac{1+r_{fh}}{1-r_{fh}} + \frac{1+r_{fc}}{1-r_{fc}}}, \quad (22)$$

which is different from the Casimir limit, due to the interface effect. Figure 5 illustrates the temperature distributions in the cross-plane nanofilms in this case. Here, we assume that the heat sinks are made of germanium (Ge) and the nanofilm is made of silicon (Si). Referring to Chen’s work [32], we have $C_{V_Si} = 0.93 \times 10^6 \text{J/m}^3\text{K}$, $\rho_{Si} = 2330 \text{kg/m}^3$, $v_{g_Si} = 1804 \text{m/s}$, $\text{MFP}_{Si} = 260.4 \text{nm}$, $C_{V_Ge} = 0.87 \times 10^6 \text{J/m}^3\text{K}$, $\rho_{Ge} = 5500 \text{kg/m}^3$, $v_{g_Ge} = 1042 \text{m/s}$, and $\text{MFP}_{Ge} = 198.6 \text{nm}$. Then, the corresponding transmissivity and reflectivity are calculated by the DMM, Eq. (17). In this case,

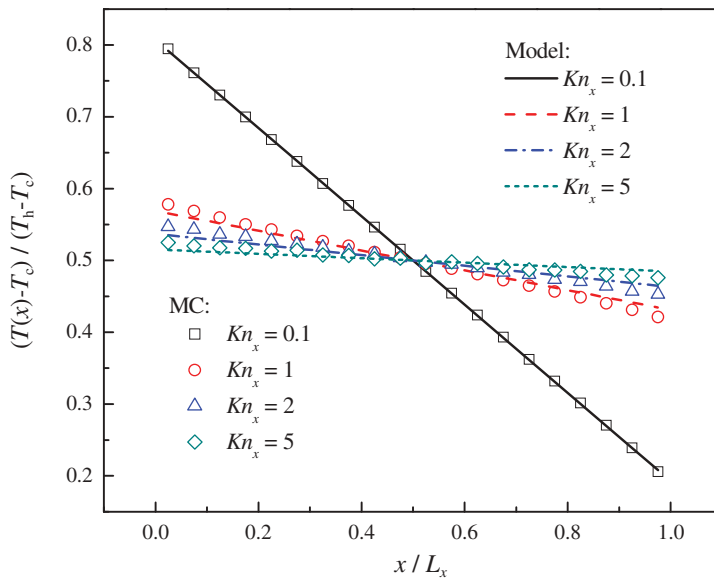


Figure 5. Temperature distributions in cross-plane nanofilms with interface effects.

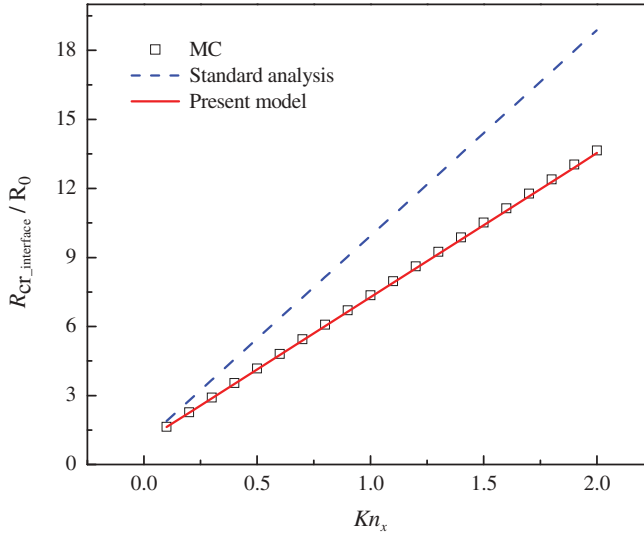


Figure 6. Cross-plane thermal resistance of nanofilms with interface effects.

both the ballistic transport and interfacial resistance can cause the boundary temperature jumps, which are enhanced with increasing Knudsen number. In addition, the model Eq. (21) can well predict the results obtained by MC simulations.

Furthermore, according to Eqs. (8) and (21), we can derive the total cross-plane thermal resistance,

$$R_{\text{cr-interface}} = \frac{L_x}{k_0} \left[1 + \frac{2}{3} Kn_x \left(\frac{1+r_{\text{fh}}}{1-r_{\text{fh}}} + \frac{1+r_{\text{fc}}}{1-r_{\text{fc}}} \right) \right] = R_0 + R_{\text{coup}}, \quad (23)$$

in which R_{coup} is the thermal resistance resulting from ballistic transport and interface effects. Figure 6 shows the cross-plane thermal resistances calculated by the model and MC simulations, respectively. Due to the interface effect, the thermal resistance is significantly enhanced compared to that with the ideal boundaries, and it increases with increasing Knudsen number. In addition, the model Eq. (23) can well predict the thermal resistances obtained by MC simulations, and the deviation between them is less than 5%.

For comparison, we also calculate the total thermal resistance by the standard analysis based on Fourier's law, which is given by

$$R_{\text{Fo}} = R_h + R_c + \frac{L_x}{k_{\text{eff}}(L_x)}, \quad (24)$$

where $R_h = 4/[(1-r_{\text{fh}})C_v v_g]$ and $R_c = 4/[(1-r_{\text{fc}})C_v v_g]$ are the interfacial resistances calculated by the DMM, and k_{eff} is the effective thermal conductivity, which can concern the size effects due to the ballistic transport or boundary scattering. The effective thermal conductivity of cross-plane nanofilms could be calculated as $k_{\text{eff}} = k_0/(1 + 4/3Kn_x)$ [13] and thus the total resistance is rewritten as

$$R_{\text{Fo}} = \frac{L_x}{k_0} \left[1 + \frac{4}{3} Kn_x + \frac{4}{3} \frac{Kn_x}{1-r_{\text{fh}}} + \frac{4}{3} \frac{Kn_x}{1-r_{\text{fc}}} \right], \quad (25)$$

which could be regarded as a summation of the diffusive, ballistic, and interfacial resistances. Importantly, in the standard analysis, the influence of interfacial resistance is localized at the

interface and thus is decoupled from the ballistic effect. As shown in [Figure 6](#), the standard analysis considerably overpredicts the thermal resistances calculated by MC simulations. In fact, referring to [Eq. \(23\)](#), the ballistic transport and interface effects are coupled in the ballistic–diffusive heat conduction, whereas the standard analysis, where the interface effect has been treated as a single interfacial resistance, ignores this interface–ballistic coupling effect. Actually, the time-domain thermoreflectance experiments by Wilson and Cahill [21] have demonstrated two features inconsistent with the standard interfacial resistance analysis; that is, the dependence of the interface resistance on the periodic heating frequency and the significant differences between the interfacial resistances of Si versus $\text{Si}_{0.99}\text{Ge}_{0.01}$. In order to explain this, Wilson and Cahill [21] proposed that the interfacial resistance should depend on the phonon MFPs in the ballistic–diffusive heat conduction, indicating the interface–ballistic coupling effect indeed. In addition, Liang et al. [35] highlighted the effects of film thickness and roughness on the thermal transport through an interface by molecular dynamics simulations, further indicating the invalidity of the standard interfacial resistance analysis. In fact, the interface–ballistic coupling effect should be critically important in practice, especially for experimental data analyses. For example, in the experiments of Raja et al. [36], the authors intended to identify the thermal ballistic transport in smooth Si nanowires by measuring the length-dependent thermal conductivity, where the interfaces between the samples and the supporting beams became a critical issue; therefore, the authors proposed that the influence of the contact resistance could be calculated as the intercept of a best fit line to the total thermal resistance, and then the actual thermal conductivity of the nanowires could be obtained by subtracting the fitting contact resistance from the total one. However, the experimental data analysis method proposed by Raja et al. [36] should merely be right for a purely diffusive heat conduction and may be inapplicable in the ballistic–diffusive regime due to the interface–ballistic coupling effects. According to [Eq. \(23\)](#), the ballistic transport–induced thermal resistance is coupled with the interfacial resistance; that is, R_{coup} . Thus, subtracting the fitting contact resistance could eliminate the influence resulting from both the ballistic transport and the interface effects. This may also be why Raja et al. [36] did not find the ballistic thermal transport across O (100) nanometer length scales even in smooth Si nanowires.

Boundary heat flux slip

Boundary heat flux slip in suspended nanofilm

The boundary heat flux slip, induced by the lateral confinement, is another important slip boundary condition in ballistic–diffusive heat conduction. The heat flux slip in a suspended in-plane nanofilm has been characterized by using the phonon BTE [4, 5, 17, 20]. In this case, the length in the x -direction is assumed to be much larger than the phonon MFP, whereas the y -directional width is comparable to the MFP. The phonon BTE is thus given by [17]

$$v_{gwy}\tau_{\omega} \frac{\partial \Delta f_{\omega}}{\partial y} + \Delta f_{\omega} = -v_{gwx}\tau_{\omega} \frac{\partial f_{\omega 0}}{\partial T} \frac{dT}{dx}, \quad (26)$$

with boundary conditions

$$\begin{aligned} \Delta f_{\omega}(0, v_{gwy} > 0) &= P\Delta f_{\omega}(0, v_{gwy} < 0), \\ \Delta f_{\omega}(L_y, v_{gwy} < 0) &= P\Delta f_{\omega}(L_y, v_{gwy} > 0), \end{aligned} \quad (27)$$

where $\Delta f_{\omega} = f_{\omega} - f_{0\omega}$; P is the phonon specularity parameter, which depends on the boundary roughness [22], $P = \exp(-16\pi^2\Delta^2/\lambda^2)$, in which Δ is the root mean square value of the roughness fluctuations; and λ is phonon wavelength. Because the in-plane nanofilm is suspended, the lateral boundaries are adiabatic, and all of the phonons striking on them should be reflected back.

By using the methodology proposed by Ziman [22], [Eq. \(25\)](#) has a solution as

$$\Delta f_{\omega} = \begin{cases} \left(v_{g\omega x} \tau_{\omega} \frac{\partial f_0}{\partial T} \frac{dT}{dx} \right) \left(\frac{1-P}{1-P \exp(-L_y/v_{g\omega y} \tau_{\omega})} \exp\left(-\frac{y}{v_{g\omega y} \tau_{\omega}}\right) - 1 \right) v_{g\omega y} > 0 \\ \left(v_{g\omega x} \tau_{\omega} \frac{\partial f_0}{\partial T} \frac{dT}{dx} \right) \left(\frac{1-P}{1-P \exp(L_y/v_{g\omega y} \tau_{\omega})} \exp\left(\frac{L_y-y}{v_{g\omega y} \tau_{\omega}}\right) - 1 \right) v_{g\omega y} < 0 \end{cases} \quad (28)$$

The heat flux distribution is calculated as

$$q(y) = \int_0^{2\pi} d\varphi \int_{-1}^1 d\mu \int \hbar \omega v_{g\omega x} D(\omega) d\omega \Delta f_{\omega}. \quad (29)$$

By using the Debye approximation, we have

$$\frac{q(y)}{q_0} = 1 - \frac{3}{4} \int_0^1 \frac{1-P}{1-P \exp\left(-\frac{1}{\mu Kn_y}\right)} \left[\exp\left(-\frac{y/L_y}{\mu Kn_y}\right) + \exp\left(-\frac{1-y/L_y}{\mu Kn_y}\right) \right] (1-\mu^2) d\mu, \quad (30)$$

where $Kn_y = l_0/L_y$ is the Knudsen number, and $q_0 = -k_0 dT/dx$ is the benchmark heat flux calculated by Fourier's law. **Figure 7** shows the heat flux distributions for the in-plane heat conduction in suspended nanofilms. The good agreement between MC simulations and the model Eq. (30), have been achieved. It is found that due to the diffusive phonon boundary scattering, the heat flux is reduced near the boundaries, and the completely specular boundary scattering ($P = 1$) will not cause the boundary heat flow slip in this case. In addition, with increasing Knudsen number, Kn_y , the influence of boundary scattering is enhanced, reducing the heat flux.

Additionally, referring to Eq. (30), the in-plane thermal resistance is given by [17]

$$R_{in} = \frac{L_x}{k_0 L_y} \left[1 - \frac{3Kn_y(1-P)}{2} \int_0^1 \frac{1 - \exp\left(-\frac{1}{\mu Kn_y}\right)}{1 - P \exp\left(-\frac{1}{\mu Kn_y}\right)} (1-\mu^2) \mu d\mu \right]^{-1}, \quad (31)$$

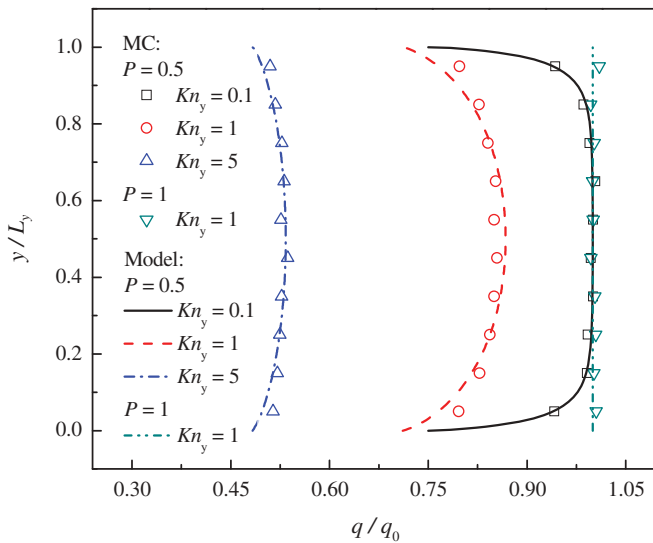


Figure 7. Heat flux distributions for in-plane heat conduction in suspended nanofilms.

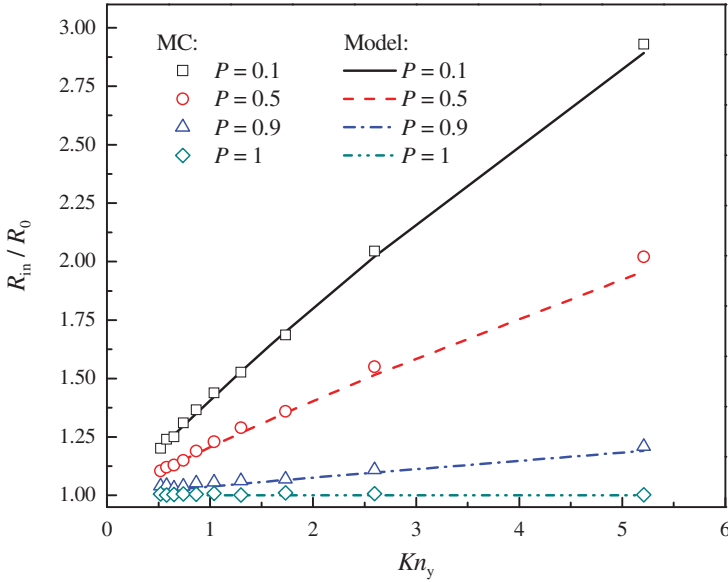


Figure 8. In-plane thermal resistance of suspended nanofilms.

in which L_x/k_0L_y is the benchmark thermal resistance predicted by Fourier's law. Actually, Eq. (31) is a transform of the widely used Fuchs-Sondheimer formula [17, 19]. Figure 8 shows the in-plane thermal resistance of the suspended nanofilms. The predictions of Eq. (31) well agree with those obtained by MC simulations. The in-plane resistance increases with increasing Knudsen number (Kn_y) or decreasing specularity parameter (P). As $P = 1$, the specular boundary scattering does not cause the boundary heat flux slip, and the in-plane thermal resistance will not be reduced by the lateral confinement, and it becomes independent on the Knudsen number Kn_y . Nevertheless, we note that the conclusion that the purely specular boundary scattering does not increase the thermal resistance is only valid for some typical nanostructures such as films and wires; Hua and Cao [37] demonstrated that it could also reduce the thermal conductivity (i.e., increase the thermal resistance) for nanoporous films.

Boundary heat flux slip in nanofilm on substrate

The interface effect induced by the substrate is a significant issue that could impact the heat flux distribution within an in-plane nanofilm on substrate, as shown in Figure 2b. The phonons in the nanofilm on the substrate can scatter at the interface as in the case of the suspended nanofilm; in addition, they can pass through the interface and enter the substrate; at the same time, the phonons in the substrate can also enter the nanofilm. In this case, two main factors could affect the heat flux distribution within the nanofilms on a substrate [24]: phonon reflection at the boundary as well as the interface and perturbation of the phonon distribution function induced by the substrate. Then, the phonon BTEs for the nanofilm labeled by "a" and the substrate labeled by "b" are given by

$$v_{g\omega ya}\tau_{\omega a}\frac{\partial \Delta f_{\omega a}}{\partial y} + \Delta f_{\omega a} = -v_{g\omega xa}\tau_{\omega a}\frac{\partial f_{\omega 0a}}{\partial T}\frac{dT}{dx}, \quad (32)$$

and

$$v_{g\omega yb} \tau_{\omega b} \frac{\partial \Delta f_{\omega b}}{\partial y} + \Delta f_{\omega b} = -v_{g\omega xb} \tau_{\omega b} \frac{\partial f_{\omega 0b}}{\partial T} \frac{dT}{dx}, \quad (33)$$

with the interface and boundary conditions [24, 38]

$$\begin{aligned} \Delta f_{\omega a}(L_{ya}, v_{g\omega ya} < 0) &= P_a \Delta f_{\omega a}(L_{ya}, v_{g\omega ya} > 0); \\ \Delta f_{\omega a}(0, v_{g\omega ya} > 0) &= P_{ab} [r_{aa} \Delta f_{\omega a}(0, v_{g\omega ya} < 0) + t_{ba} \Delta f_{\omega b}(0, v_{g\omega yb} > 0)], \\ \Delta f_{\omega b}(0, v_{g\omega yb} < 0) &= P_{ab} [r_{bb} \Delta f_{\omega b}(0, v_{g\omega yb} > 0) + t_{ab} \Delta f_{\omega a}(0, v_{g\omega ya} < 0)]; \\ \Delta f_{\omega b}(-L_{yb}, v_{g\omega yb} > 0) &= 0. \end{aligned} \quad (34)$$

where r_{aa} and r_{bb} are the reflection coefficients at the interface; t_{ab} and t_{ba} are the transmission coefficients; and P_a and P_{ab} are the specularly parameters. Because the substrate is generally thicker than the nanofilm and holds the short phonon MFPs, the interface/boundary effects could be non-significant in the substrate. Therefore, we focus on the heat flux distribution within the nanofilms and the remote boundary of the substrate is assumed to be completely diffusive for simplicity.

Then, we can derive the solutions of the phonon BTEs above:

$$\Delta f_{\omega a} = \begin{cases} v_{g\omega xa} \tau \frac{\partial f_{\omega 0a}}{\partial T} \frac{dT}{dx} \left(G_a^+ \exp\left(-\frac{y}{v_{g\omega ya} \tau_{\omega a}}\right) - 1 \right) v_{g\omega ya} > 0 \\ v_{g\omega xa} \tau \frac{\partial f_{\omega 0a}}{\partial T} \frac{dT}{dx} \left(G_a^- \exp\left(\frac{y}{v_{g\omega ya} \tau_{\omega a}}\right) - 1 \right) v_{g\omega ya} < 0 \end{cases}, \quad (35)$$

with

$$\begin{aligned} G_a^+ &= \frac{1 + P_{ab} \left[\left(\exp\left(-\frac{L_{ya}}{l_{\omega a} \mu}\right) (1 - P_a) - 1 \right) r_{aa} + \left(\exp\left(-\frac{L_{yb}}{l_{\omega b} \mu}\right) - 1 \right) \gamma_{ab}^{-1} t_{ba} \right]}{1 - P_a P_{ab} r_{aa} \exp\left(-2\frac{L_{ya}}{l_{\omega a} \mu}\right)}, \\ G_a^- &= \exp\left(-\frac{L_{ya}}{l_{\omega a} \mu}\right) \frac{1 - P_a + P_a \exp\left(-\frac{L_{ya}}{l_{\omega a} \mu}\right) \left[1 - P_{ab} (r_{aa} + \gamma_{ab}^{-1} t_{ba}) + \exp\left(-\frac{L_{yb}}{l_{\omega b} \mu}\right) \gamma_{ab}^{-1} P_{ab} t_{ba} \right]}{1 - P_a P_{ab} r_{aa} \exp\left(-2\frac{L_{ya}}{l_{\omega a} \mu}\right)}, \end{aligned} \quad (36)$$

and

$$\Delta f_{\omega b} = \begin{cases} v_{g\omega xb} \tau \frac{\partial f_{\omega 0b}}{\partial T} \frac{dT}{dx} \left(G_b^+ \exp\left(-\frac{y}{v_{g\omega yb} \tau_{\omega b}}\right) - 1 \right) v_{g\omega yb} > 0 \\ v_{g\omega xb} \tau \frac{\partial f_{\omega 0b}}{\partial T} \frac{dT}{dx} \left(G_b^- \exp\left(\frac{y}{v_{g\omega yb} \tau_{\omega b}}\right) - 1 \right) v_{g\omega yb} < 0 \end{cases}, \quad (37)$$

with

$$\begin{aligned} G_b^+ &= \exp\left(-\frac{L_{yb}}{l_{\omega b} \mu}\right), \\ G_b^- &= \frac{1 - P_{ab} \left[r_{bb} + \gamma_{ab} t_{ab} + \exp\left(-2\frac{L_{ya}}{l_{\omega a} \mu} - \frac{L_{yb}}{l_{\omega b} \mu}\right) P_a P_{ab} (r_{aa} r_{bb} - t_{ab} t_{ba}) - \exp\left(-\frac{L_{ya}}{l_{\omega a} \mu}\right) \gamma_{ab} (1 - P_a) t_{ab} \right. \\ &\quad \left. - \exp\left(-2\frac{L_{ya}}{l_{\omega a} \mu}\right) P_a (\gamma_{ab} t_{ab} - r_{aa} + P_{ab} (r_{aa} r_{bb} - t_{ab} t_{ba})) - r_{bb} \exp\left(-\frac{L_{yb}}{l_{\omega b} \mu}\right) \right]}{1 - P_a P_{ab} r_{aa} \exp\left(-2\frac{L_{ya}}{l_{\omega a} \mu}\right)}, \end{aligned} \quad (38)$$

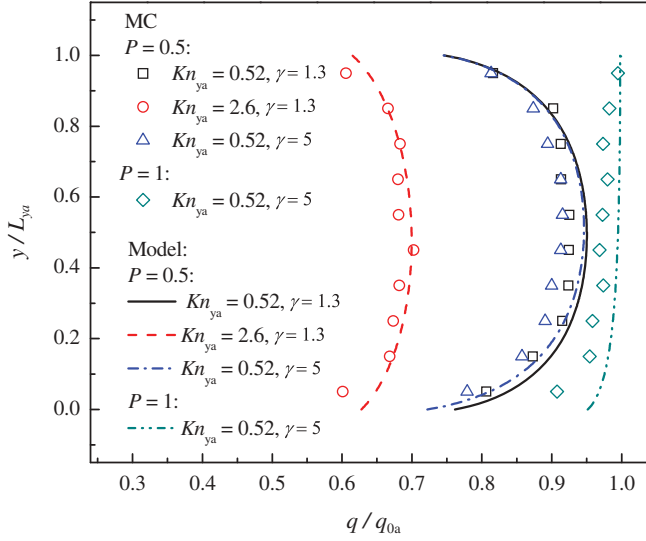


Figure 9. Heat flux distributions for in-plane heat conduction in nanofilms on a substrate.

in which $l_{\omega a} = v_{g\omega a} \tau_{\omega a}$ and $l_{\omega b} = v_{g\omega b} \tau_{\omega b}$ are the phonon MFPs for the nanofilm and the substrate, respectively, and the MFP ratio is $\gamma_{ab} = l_{\omega a} / l_{\omega b}$.

Furthermore, by using the Debye approximation, the heat flux distribution within the nanofilm ($0 \leq y < L_{ya}$) is written as

$$\frac{q_a(y)}{q_{0a}} = 1 - \frac{3}{4} \int_0^1 \left(G_a^+ \exp\left(-\frac{y/L_{ya}}{\mu Kn_{ya}}\right) + G_a^- \exp\left(\frac{y/L_{ya}}{\mu Kn_{ya}}\right) \right) (1 - \mu^2) d\mu, \quad (39)$$

in which $Kn_{ya} = l_{0a} / L_{ya}$ is the Knudsen number, l_{0a} is the average phonon MFP, and the benchmark heat flux, q_{0a} , is equal to $-k_{0a} dT/dx$.

Figure 9 shows the heat flux distributions within the in-plane nanofilms on a substrate. The nanofilm and the substrate are assumed to be made of Si and Ge, respectively. The MFP ratio is $\gamma = \text{MFP}_{\text{Si}} / \text{MFP}_{\text{Ge}} = 1.3$, and the reflectivity and transmissivity—that is, r_{aa} , r_{bb} , t_{ab} , and t_{ba} —can also be estimated by using the phonon properties of Si and Ge [32]. For phonons' specular transmission and reflection at the interface, the acoustic mismatch model is generally employed to calculate the angle-dependent transmissivity and reflectivity [39]. In fact, the reflection and transmission at the interface could be a complicated process; for example, the effects of the phonon mode conversion [40] and the strength of the bond between the atoms at the interface [41] could affect them. For simplicity, we further introduce a few assumptions into both the model and the simulations. Mode conversion at the interface is ignored, which has been proven to be a good approximation [32]. The average integrated specular transmissivity and reflectivity, which are angle independent, are calculated by using Prasher's method [41]; that is,

$$\begin{aligned} \bar{t}_{\text{Si-Ge(Ge-Si)}} &= 2 \int_0^{\theta_c} t_{\text{Si-Ge(Ge-Si)}} \cos(\theta) d \cos(\theta), \\ \bar{r}_{\text{Si-Ge(Ge-Si)}} &= 1 - \bar{t}_{\text{Si-Ge(Ge-Si)}} \end{aligned} \quad (40)$$

with

$$t_{\text{Si-Ge(Ge-Si)}} = \frac{4z_{\text{Si}}z_{\text{Ge}} \cos(\theta_{\text{Si}}) \cos(\theta_{\text{Ge}})}{[z_{\text{Si}} \cos(\theta_{\text{Si}}) + z_{\text{Ge}} \cos(\theta_{\text{Ge}})]^2}, \quad (41)$$

in which $z_{\text{Si}} = \rho_{\text{Si}}v_{\text{g-Si}}$, $z_{\text{Ge}} = \rho_{\text{Ge}}v_{\text{g-Ge}}$, and $\sin(\theta_{\text{Si}})/v_{\text{g-Si}} = \sin(\theta_{\text{Ge}})/v_{\text{g-Ge}}$. In addition, referring to Chen's paper [32], when using the acoustic mismatch model, due to the energy balance requirement, a modification of the transmissivity should be adopted; that is, $\bar{t}'_{\text{Si-Ge}} = \bar{t}_{\text{Ge-Si}}(v_{\text{g-Ge}}C_{V\text{-Ge}}/v_{\text{g-Si}}C_{V\text{-Si}})$ and $\bar{r}'_{\text{Si-Ge}} = 1 - \bar{r}_{\text{Si-Ge}}$. According to Figure 9, the heat flux is also reduced near the boundary and the interface, and this heat flux slip phenomenon is enhanced with increasing Kn_{ya} , as in the case of the suspended nanofilms. However, the interface effect indeed indicates some differences. The heat flux distribution becomes asymmetrical due to the perturbation of the phonon distribution function near the interface. If we increase the MFP ratio, γ , from 1.3 to 5, the heat flux near the interface is further reduced. As $P = 1$ —that is, the diffusive boundary scattering is completely eliminated—the heat flux distribution within the suspended nanofilms becomes a linear function, whereas the heat flux is still affected by the interface in the nanofilms on the substrate. In addition, the present model can fairly well characterize the heat flux distribution within the nanofilms on a substrate compared to MC simulations, though some deviations could exist.

Furthermore, using Eq. (39), the thermal resistance of the nanofilm on a substrate is obtained:

$$R_{\text{in-interface}} = R_{0a} \left\{ 1 - \frac{3Kn_{\text{ya}}}{4} \int_0^1 (G_a^+ + G_a^-) \left(1 - \exp\left(-\frac{1}{\mu Kn_{\text{ya}}}\right) \right) (1 - \mu^2) \mu d\mu \right\}^{-1}, \quad (42)$$

in which $R_{0a} = L_x/(k_{0a}L_{\text{ya}})$ is the benchmark thermal resistance based on Fourier's law. We note that in the theoretical frame based on Fourier's law, the thermal resistance of the nanofilms on a substrate should be identical to that of the suspended nanofilms, because there will be no net heat flux through the interface. In contrast, in the ballistic-diffusive heat conduction, both the boundary scattering and the interface effect could affect the thermal resistance. The influence of the boundary scattering on the thermal resistance of the in-plane suspended nanofilms has been well described by the Fuchs-Sondheimer formula [4, 17]; a model beyond the Fuchs-Sondheimer formula, which can

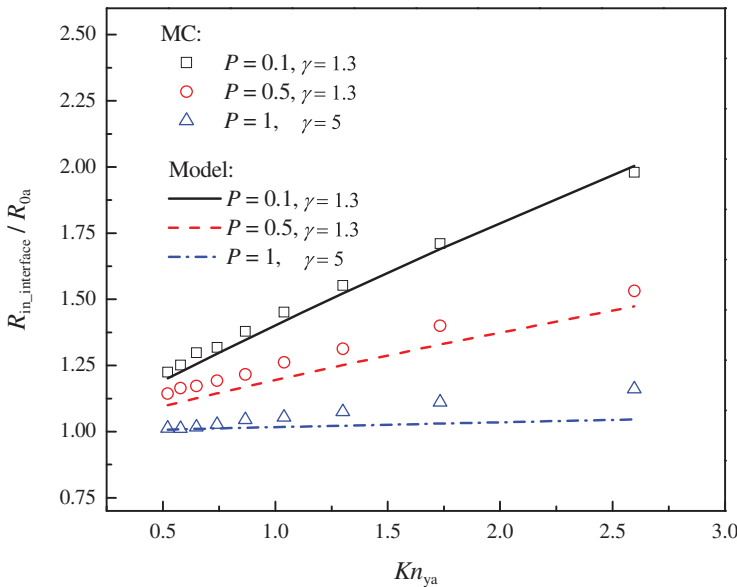


Figure 10. In-plane thermal resistance of nanofilms on a substrate.

address both boundary scattering and interface (substrate) effects, is indeed needed, such as in the case of supporting graphene [27]. Figure 10 compares the in-plane thermal resistances of the nanofilms on a substrate calculated by the model and MC simulations, respectively. The thickness of the nanofilms (L_{ya}) ranges from 100 to 500 nm, and the thickness of the substrate (L_{yb}) is set as 500 nm. It is found that the thermal resistance increases with increasing Knudsen number (Kn_{ya}), decreasing specularly parameter (P), or increasing MFP ratio (γ). Importantly, even when $P = 1$, the interface effect alone can also increase the in-plane thermal resistance. In addition, the present model can well predict the results by MC simulations, especially as P is small, and the maximum deviation is less than 20%.

Conclusions

In ballistic–diffusive heat conduction, interactions between phonons and boundaries (or interfaces) can cause two kinds of slip boundary conditions: boundary temperature jump and boundary heat flux slip. In the present work, we used the phonon BTE and the phonon tracing MC method to study these two slip boundary conditions in nanofilms on a substrate. The thermal transport in nanofilms has generally been clarified into two typical types; that is, cross-plane heat conduction and in-plane heat conduction. In the cross-plane case where the boundary temperature jump is the dominant non-Fourier phenomenon, ballistic transport leads to temperature jumps and thus introduces ballistic thermal resistance; in addition, both the boundary temperature jump and the cross-plane thermal resistance increase with increasing Knudsen number. When considering interface effects, the temperature jump and the total thermal resistance are both enhanced, and the interface–ballistic coupling effect was identified, indicating the inapplicability of the standard thermal resistance analysis. In addition, the boundary temperature jump model considering interface effects was derived from the phonon BTE, and it was verified by comparison with MC simulations. In contrast, the in-plane heat conduction is controlled by the boundary heat flux slip. Both the phonon boundary scattering and perturbation of phonon distribution function induced by interface could cause heat flux slip, leading to a variation in in-plane thermal resistance. Even as the diffusive boundary scattering is completely eliminated—that is, $P = 1$ —the interface effect alone could also cause the heat flux slip as well as a change in in-plane thermal resistance. Furthermore, a model beyond the Fuchs-Sondheimer formula, which addresses both boundary scattering and interface effects, was obtained from the phonon BTE, and good agreement with our MC simulations indicates its validity. Our work has highlighted the interface effects on the slip boundary conditions in ballistic–diffusive heat conduction and can provide a more in-depth understanding as well as some analytical models for predicting and controlling nanoscale thermal transport.

Funding

This work is financially supported by the National Natural Science Foundation of China (Nos. 51676108, 51356001), Science Fund for Creative Research Group (No. 51621062), and the Tsinghua National Laboratory for Information Science and Technology of China (TNList).

References

1. E. Pop, Energy Dissipation and Transport in Nanoscale Devices, *Nano Research*, Vol. 3, pp. 147–169, 2010.
2. D.G. Cahill, P.V. Braun, G. Chen, et al., Nanoscale Thermal Transport. II. 2003–2012, *Applied Physics Letters*, Vol. 1, pp. 011305-1–45, 2014.
3. R. Chen, A.I. Hochbaum, P. Murphy, et al., Thermal Conductance of Thin Silicon Nanowires, *Physical Review Letters*, Vol. 101, pp. 105501-1–4, 2008.
4. X. Wang and B. Huang, Computational Study of In-Plane Phonon Transport in Si Thin Films, *Scientific Reports*, Vol. 4, pp. 6399-1–9, 2014.

5. Y.C. Hua and B.Y. Cao, Ballistic–Diffusive Heat Conduction in Multiply-Constrained Nanostructures, *International Journal of Thermal Sciences*, Vol. 101, pp. 126–132, 2016.
6. Y.C. Hua and B.Y. Cao, Phonon Ballistic–Diffusive Heat Conduction in Silicon Nanofilms by Monte Carlo Simulations, *International Journal of Heat and Mass Transfer*, Vol. 78, pp. 755–759, 2014.
7. J. Maassen and M. Lundstrom, Steady-State Heat Transport: Ballistic-to-Diffusive with Fourier’s Law, *Journal of Applied Physics*, Vol. 117, pp. 035104-1–8, 2015.
8. J. Maassen and M. Lundstrom, A Simple Boltzmann Transport Equation for Ballistic to Diffusive Transient Heat Transport, *Journal of Applied Physics*, Vol. 117, pp. 135102-1–9, 2015.
9. J.M. Péraud and N.G. Hadjiconstantinou, Extending the Range of Validity of Fourier’s Law into the Kinetic Transport Regime via Asymptotic Solution of the Phonon Boltzmann Transport Equation, *Physical Review B*, Vol. 93, No. 4, pp. 045424-1–21, 2016.
10. J. Kaiser, T. Feng, J. Maassen, et al., Thermal Transport at the Nanoscale: A Fourier’s Law vs. Phonon Boltzmann Equation Study, *Journal of Applied Physics*, Vol. 121, pp. 044302-1–23, 2017.
11. P.A. Thompson and S.M. Troian, A General Boundary Condition for Liquid Flow at Solid Surfaces, *Nature*, Vol. 389, pp. 360–362, 1997.
12. Z. Rieder, J.L. Lebowitz, and E. Lieb, Properties of a Harmonic Crystal in a Stationary Nonequilibrium State, *Journal of Mathematical Physics*, Vol. 8, pp. 1073–1078, 1967.
13. A. Majumdar, Microscale Heat Conduction in Dielectric Thin Films, *Journal of Heat Transfer*, Vol. 115, pp. 7–16, 1993.
14. J.W. Jiang, J. Chen, J.S. Wang, and B. Li, Edge States Induce Boundary Temperature Jump in Molecular Dynamics Simulation of Heat Conduction, *Physical Review B*, Vol. 80, pp. 052301-1–4, 2009.
15. D.P. Sellan, J.E. Turney, A.J.H. McGaughey, et al., Cross-Plane Phonon Transport in Thin Films, *Journal of Applied Physics*, Vol. 108, pp. 113524-1–8, 2010.
16. Y.C. Hua and B.Y. Cao, The Effective Thermal Conductivity of Ballistic–Diffusive Heat Conduction in Nanostructures with Internal Heat Source, *International Journal of Heat and Mass Transfer*, Vol. 92, pp. 995–1003, 2016.
17. J.E. Turney, A.J.H. McGaughey, and C.H. Amon, In-Plane Phonon Transport in Thin Films, *Journal of Applied Physics*, Vol. 107, 024317-1–8, 2010.
18. A. Sellitto, F.X. Alvarez, and D. Jou, Temperature Dependence of Boundary Conditions in Phonon Hydrodynamics of Smooth and Rough Nanowires, *Journal of Applied Physics*, Vol. 107, No. 11, pp. 114312-1–7, 2010.
19. J.-P.M. Péraud and N.G. Hadjiconstantinou, Efficient Simulation of Multidimensional Phonon Transport Using Energy-Based Variance-Reduced Monte Carlo Formulations, *Physical Review B*, Vol. 84, pp. 205331-1–15, 2011.
20. M. Xu, Slip Boundary Condition of Heat Flux in Knudsen Layers, *Proceedings of the Royal Society A*, Vol. 470, pp. 20130578-1–9, 2014.
21. R.B. Wilson and D.G. Cahill, Anisotropic Failure of Fourier Theory in Time-Domain Thermoreflectance Experiments, *Nature Communications*, Vol. 5, pp. 5075–6075, 2014.
22. J. Ziman, *Electrons and Phonons*, Oxford University Press, London, 1961.
23. P. Martin, Z. Aksamija, E. Pop, and U. Ravaioli, Impact of Phonon–Surface Roughness Scattering on Thermal Conductivity of Thin Si Nanowires, *Physical Review Letters*, Vol. 102, pp. 125503-1–4, 2009.
24. P. Rennert and A. Brzezinski, Solution of the Boltzmann Equation for Multilayer Systems, *Physical Review B*, Vol. 52, pp. 1612–1617, 1995.
25. G. Chen, Size and Interface Effects on Thermal Conductivity of Superlattices and Periodic Thin-Film Structures, *Journal of Heat Transfer*, Vol. 119, pp. 220–229, 1997.
26. B. Qiu and X. Ruan, Reduction of Spectral Phonon Relaxation Times from Suspended to Supported Graphene, *Applied Physics Letters*, Vol. 100, pp. 193101-1–4, 2012.
27. M.M. Sadeghia, I. Joa, and L. Shi, Phonon–Interface Scattering in Multilayer Graphene on an Amorphous Support, *Proceedings of the National Academy of Sciences (PNAS)*, Vol. 110, pp. 16321–16326, 2013.
28. X. Zhang, H. Bao, and M. Hu, Bilateral Substrate Effect on the Thermal Conductivity of Two-Dimensional Silicon, *Nanoscale*, Vol. 7, pp. 6014–6022, 2015.
29. J.P.M. Péraud and N.G. Hadjiconstantinou, An Alternative Approach to Efficient Simulation of Micro/Nanoscale Phonon Transport, *Applied Physics Letters*, Vol. 101, pp. 153114-1–4, 2012.
30. Y.C. Hua and B.Y. Cao, An Efficient Two-Step Monte Carlo Method for Heat Conduction in Nanostructures, *Journal of Computational Physics*, Vol. 342, pp. 253–266, 2017.
31. D.S. Tang, Y.C. Hua, and B.Y. Cao, Thermal Wave Propagation through Nanofilms in Ballistic–Diffusive Regime by Monte Carlo Simulations, *International Journal of Thermal Sciences*, Vol. 109, pp. 81–89, 2016.
32. G. Chen, Thermal Conductivity and Ballistic–Phonon Transport in the Cross-Plane Direction of Superlattices, *Physical Review B*, Vol. 57, pp. 14958–14973, 1998.
33. R. Prasher, Transverse Thermal Conductivity of Porous Materials Made from Aligned Nano- and Microcylindrical Pores, *Journal of Applied Physics*, Vol. 100, pp. 064302-1–7, 2006.

34. A.C. Cogley, S.E. Gilles, and W.G. Vincenti, Differential Approximation for Radiative Transfer in a Nongrey Gas Near Equilibrium, *AIAA Journal*, Vol. 6, pp. 551–553, 1968.
35. Z. Liang, K. Sasikumar, and P. Keblinski, Thermal Transport across a Substrate–Thin-Film Interface: Effects of Film Thickness and Surface Roughness, *Physical Review Letters*, Vol. 113, pp. 065901-1–5, 2014.
36. S.N. Raja, R. Rhyner, K. Vuttivorakulchai, et al., Length Scale of Diffusive Phonon Transport in Suspended Thin Silicon Nanowires, *Nano Letters*, Vol. 17, pp. 276–283, 2017.
37. Y.C. Hua and B.Y. Cao, Anisotropic Heat Conduction in Two-Dimensional Periodic Silicon Nanoporous Films, *Journal of Physical Chemistry C*, Vol. 121, pp. 5293–5301, 2017.
38. R. Prasher, Thermal Conductivity of Composites of Aligned Nanoscale and Microscale Wires and Pores, *Journal of Applied Physics*, Vol. 100, pp. 034307-1–9, 2006.
39. E.T. Swartz and R.O. Pohl, Thermal Boundary Resistance, *Reviews of Modern Physics*, Vol. 61, pp. 605–668, 1989.
40. B.A. Auld, *Acoustic Fields and Waves in Solids*, 2nd ed., Krieger Publishing Company, Malabar, FL, 1990.
41. R. Prasher, Acoustic Mismatch Model for Thermal Contact Resistance of van der Waals Contacts, *Applied Physics Letters*, Vol. 94, pp. 041905-1–3, 2009.